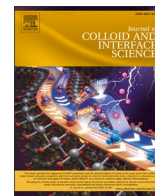




Contents lists available at ScienceDirect

Journal of Colloid And Interface Science

journal homepage: www.elsevier.com/locate/jcis

Synergistic Co-N/V-N dual sites in N-doped $\text{Co}_3\text{V}_2\text{O}_8$ nanosheets: pioneering high-efficiency bifunctional electrolysis for high-current water splitting

Mingcheng Gao^a, Zhiyang Huang^a, Lixia Wang^a, Huatong Li^a, Changping Ruan^{a,*},
Raeid Sadeq^b, Tayirjan Taylor Isimjan^{b,*}, Xiulin Yang^{a,*}

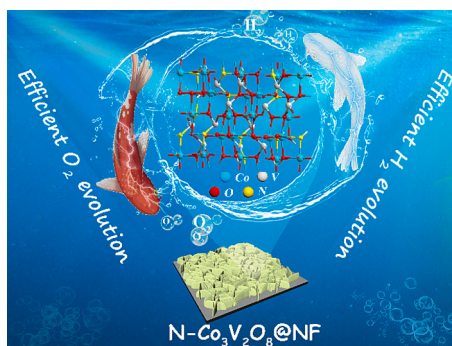
^a Guangxi Key Laboratory of Low Carbon Energy Materials, School of Chemistry and Pharmaceutical Sciences, Guangxi Normal University, Guilin 541004, China

^b Saudi Arabia Basic Industries Corporation (SABIC) at King Abdullah University of Science and Technology (KAUST), Thuwal 23955-6900, Saudi Arabia

HIGHLIGHTS

- Sheet-like $\text{N-Co}_3\text{V}_2\text{O}_8@\text{NF}$ is constructed by an impregnation-thermal nitridation strategy.
- The catalyst exhibits supernormal HER ($\eta_{10} = 63 \text{ mV}$) and OER ($\eta_{10} = 256 \text{ mV}$) activity.
- The overall water splitting exhibits ultra-low cell voltage ($1.97 \text{ V}@500 \text{ mA cm}^{-2}$).
- The conductivity, hydrophilicity and formed Co-N/V-N dual active sites dominate the superior performance.

GRAPHICAL ABSTRACT



ARTICLE INFO

Keywords:

$\text{N-Co}_3\text{V}_2\text{O}_8@\text{NF}$
Nitrogen doping
Dual active sites
Bifunctional electrocatalysts
Water splitting

ABSTRACT

Developing affluent dual-metal active sites bifunctional electrocatalysts for hydrogen evolution reaction (HER) and oxygen evolution reaction (OER) is essential to achieve large-scale water electrolysis, whereas still remains challenging. Herein, a novel nitrogen-doped cobalt-vanadium oxide with abundant Co-N and V-N dual active sites supported on nickel foam ($\text{N-Co}_3\text{V}_2\text{O}_8@\text{NF}$) is constructed by a controllable impregnation-thermal nitridation strategy. The staggered nanosheet structure ensures optimal exposure of active sites. More importantly, N doping effectively regulates the electronic structure of the metal centers and induces the formation of Co-N and V-N dual active sites, which is conducive to improving the conductivity and hydrophilicity, thus synergistically enhancing the electrocatalytic efficiency. Consequently, the optimized $\text{N-Co}_3\text{V}_2\text{O}_8@\text{NF}$ exhibits prominent HER ($63 \text{ mV}@10 \text{ mA cm}^{-2}$) and OER ($256 \text{ mV}@10 \text{ mA cm}^{-2}$) activities, surpassing most contemporary bifunctional electrocatalysts. In practical application, the assembled $\text{N-Co}_3\text{V}_2\text{O}_8@\text{NF}^{(+/-)}$ electrolyzer consistently achieved ultra-low cell voltages of 1.97 and 2.03 V at 500 and 1000 mA cm^{-2} , respectively, superior to the benchmark $\text{RuO}_2@\text{NF}^{(+)}$ || $\text{Pt/C}@\text{NF}^{(-)}$ and showcasing robust durability. This paves the way for its prospective adoption in industrial water electrolysis applications.

* Corresponding authors.

E-mail addresses: cp_ruan@gxnu.edu.cn (C. Ruan), isimjant@sabic.com (T. Taylor Isimjan), xlyang@gxnu.edu.cn (X. Yang).

<https://doi.org/10.1016/j.jcis.2023.12.064>

Received 21 September 2023; Received in revised form 5 December 2023; Accepted 10 December 2023

Available online 13 December 2023

0021-9797/© 2023 Elsevier Inc. All rights reserved.

1. Introduction

Urgently developing efficient, clean and sustainable alternative energy sources to alleviate global energy and environmental problems remains a significant challenge. Electrocatalytic overall water splitting (OWS) technology is a promising and attractive approach to tackle the energy crisis [1], where the cathodic hydrogen evolution reaction (HER) and the anodic oxygen evolution reaction (OER) are two critical half-reactions [2,3]. Nevertheless, the catalytic efficiency of these catalysts is severely impeded by sluggish reaction kinetics and complex multi-electron reaction pathways [4], necessitating a substantial overpotential for both HER and OER [5]. The creation of a bifunctional electrocatalyst with superior performance not only simplifies production processes by reducing the need for different catalysts, but also prevents cross-contamination between the two reaction electrodes [6,7]. Designing such a bifunctional electrocatalyst is a formidable challenge due to the distinct reaction mechanisms of HER and OER. Therefore, the development of efficient bifunctional electrocatalysts is crucial for accelerating reaction rates and reducing overpotential [8]. Currently, noble-metal Pt/Ru-based materials are considered the benchmark catalysts for HER and OER, respectively, but their high cost, scarcity, and insufficient stability immensely restrict their widespread applications [9]. Therefore, it is extremely eager to design efficient and durable non-precious metal-based bifunctional electrocatalysts to improve the efficiency of OWS.

Recently, investigations on efficient, low-cost, and abundant electrocatalysts, especially transition metal oxides [10,11], nitrides [12], and phosphides [13] have drawn great attention to superseding Pt/Ru-based electrocatalysts due to their robust durability in alkaline media [14]. Among these, Co/Fe/Ni-based monometallic oxides have shown promising catalytic capabilities in OWS. Unfortunately, their catalytic activity is still insufficient due to the limited number of available active sites. In contrast, bimetallic oxides offer enhanced catalytic properties due to the combination of multiple active species [15]. Vanadium, being abundant and having multiple oxidation states, exhibits commendable electrochemical performance [16,17]. Co/V-based electrocatalysts, although efficacious for OER, are less explored for HER and OWS. However, the unsatisfactory catalytic activity of bimetallic oxides due to poor conductivity is a significant bottleneck in meeting the demand in practical applications [18]. Therefore, effective strategies for heteroatom doping (nonmetal doping, metal doping, and co-doping) [19], and morphology tuning (0D, 1D, 2D, 3D, and free-standing) have been developed [20,21], which have been used to further promote the rational electronic structure design. Nitrogen (N) is one of the most commonly used nonmetal dopants. On the one hand, N element can adjust the electronic structure of metal centers, thus reducing the charge transfer resistance and accelerating the reaction kinetics [22,23]. On the other hand, the formation of metal-nitrogen (M–N) bonds not only holds considerable electrical conductivity but can also serve as active sites for overall water splitting, thereby improving the catalytic performance [24,25]. However, achieving compatibility between HER and OER remains a challenge, and the use of binders (such as Nafion) to anchor powered catalysts onto conductive substrates may result in weak adhesion, high interfacial resistance, and poor stability at high current densities, thus hindering efficient water splitting [26,27]. To overcome these drawbacks, it is ideal to construct a self-supporting heteroatom-doped bifunctional catalyst with superior conductivity and abundant active sites for industrial applications.

Herein, we present a self-supported N-doped cobalt-vanadium bimetallic oxide catalyst (N-Co₃V₂O₈@NF) for both HER and OER, as well as OWS. Nitrogen incorporation can modulate the electronic structure of metal centers that generate Co-N and V-N dual active sites, and significantly enhance the conductivity and hydrophilicity, further impressively improving the catalytic activity. Specifically, the obtained N-Co₃V₂O₈@NF delivers the current density of 10 mA cm⁻² at ultra-low overpotentials of 63 and 256 mV for HER and OER, respectively.

Furthermore, the assembled two-electrode electrolyzer of N-Co₃V₂O₈@NF can achieve 10/100 mA cm⁻² at low cell voltages of 1.54/1.86 V, while maintaining long-term stability at 100 mA cm⁻² for 60 h without degradation, demonstrating its broad prospects for large-scale industrial applications.

2. Experimental section

2.1. Synthesis of ZIF-67@NF nanosheets

All experiments employed by deionized water and all reagents were of analytical grade and used directly without further purification. Following a slightly modified methodology from a previous study [28], Co-based zeolitic imidazolate framework (ZIF-67) nanosheets were fabricated. To eliminate surface impurities, a piece of NF (1 cm × 1 cm) was ultrasonically cleaned with 0.5 M H₂SO₄, ethanol, and deionized (DI) water for 15 min, respectively. Subsequently, separate solutions of 1.6 mmol Co(NO₃)₂·6H₂O and 0.8 mmol 2-MIM were prepared in 20 mL of DI water and stirred at 25 °C for 10 min. These were then combined and stirred for an additional 10 min. After immersing the NF into the above solution for 6 h. Finally, the purple ZIF-67 modified NF (tagged as ZIF-67@NF) was drawn out, washed with DI water, and vacuum-dried at 60 °C for 12 h.

2.2. Synthesis of Co₃V₂O₈@NF nanosheets

The Co₃V₂O₈@NF nanosheets were produced using the impregnation method. Briefly, ZIF-67@NF was immersed in 40 mL of 15 mg L⁻¹ NaVO₃ solution for 4 h. After the reaction was complete, the product was taken out and dried at 60 °C for 12 h. The mass loading of Co₃V₂O₈ is approximately 6.3 mg cm⁻².

2.3. Synthesis of N-Co₃V₂O₈@NF nanosheets

The N-doped Co₃V₂O₈@NF (denoted as N-Co₃V₂O₈@NF) was synthesized via thermal nitridation. Specifically, a piece of Co₃V₂O₈@NF was positioned at the center region of a tube furnace and subsequently heated at 400 °C for 3 h with a ramp rate of 5 °C min⁻¹ under NH₃ atmosphere. For comparison, the Co₃V₂O₈@NF was annealed at different nitridation temperatures of 300, 350, 450, and 500 °C (labeled as N-Co₃V₂O₈@NF-300, N-Co₃V₂O₈@NF-350, N-Co₃V₂O₈@NF-450, and N-Co₃V₂O₈@NF-500), while keeping other conditions remaining constant. The mass loading of N-Co₃V₂O₈ on NF is approximately 6 mg cm⁻².

2.4. Synthesis of N-ZIF-67@NF and N-NaVO₃@NF

As a comparison, N-ZIF-67@NF was synthesized using a method akin to N-Co₃V₂O₈@NF synthesis, but ZIF-67@NF was the nitridation precursor. For N-NaVO₃@NF production, a precleaned NF was submerged in a 40 mL solution of 15 mg L⁻¹ NaVO₃ for 4 h. Subsequently, the intermediate product was treated using the identical nitriding procedure to obtain N-NaVO₃@NF. The mass loading of N-ZIF-67 and N-NaVO₃ are approximately 5.8 and 4.1 mg cm⁻².

2.5. Synthesis of RuO₂ and Pt/C electrodes

2.0 mg of RuO₂ powder or commercial Pt/C was dispersed in the mixed solution embracing 200 μL DI water, 200 μL ethanol, and 10 μL 5 wt% Nafion. After ultrasound for 30 min, 200 μL of the above mixture was drop-casted onto the NF surface (1 cm × 1 cm) and dried in air at ambient temperature.

3. Result and discussion

3.1. Synthesis and structural analysis

As clarified in Fig. 1a, the N-Co₃V₂O₈@NF nanosheets were synthesized through impregnation and thermal nitridation. Initially, hexagonal ZIF-67 nanosheets were formed through in situ growth on the NF. Subsequently, the obtained ZIF-67@NF was immersed in a NaVO₃ solution, triggering an ion exchange reaction between Co²⁺ and VO₃⁻ resulting in the formation of Co₃V₂O₈@NF. The last step introduces the N element into Co₃V₂O₈@NF in an NH₃ atmosphere to acquire N-Co₃V₂O₈@NF nanosheets. X-ray powder diffraction (XRD) was utilized to probe the crystalline structure of as-prepared catalysts. Fig. 1b displays patterns that closely align with the standard Co₃V₂O₈ card (JCPDS: 16-0675). Besides, the structure of Co₃V₂O₈ remains intact after N doping. A noticeable feature is the more pronounced diffraction peak intensities in N-Co₃V₂O₈, hinting at enhanced crystallinity due to nitrogen doping. This increased crystallinity stems from the weaker electronegativity of nitrogen compared to oxygen, allowing nitrogen to replace some of the oxygen atoms in Co₃V₂O₈ during gas phase nitridation [29]. Additionally, the changes in XRD spectra of ZIF-67 and NaVO₃ after nitridation further underscore the impact of N doping (Fig. S2). Raman spectroscopy offers insight into the surface chemical bonds of the catalysts. As shown in Fig. 1c, the peaks at 327 and 807 cm⁻¹ are assignable to the stretching vibrations of Co-O and V-O, respectively [30,31]. Post nitrogen incorporation, two new peaks emerge at 507 and 617 cm⁻¹, corresponding to Co-N and V-N bonds, respectively [32,33], which further proves the triumphant doping of N and the formation of Co-N and V-N dual active sites. Moreover, the surface area and pore size of N-Co₃V₂O₈@NF were calculated using the N₂ adsorption-desorption isotherm. In order to perform the Brunauer-Emmett-Taylor (BET) surface area test, approximately 100 mg of N-Co₃V₂O₈ was stripped from the nickel foam substrate. As depicted in Fig. 1d, the N-Co₃V₂O₈@NF has a specific surface area of 36.3 m² g⁻¹ and an average pore size distribution of 3.8 nm. This large BET surface area, combined with its unique mesoporous structure, which promotes the electrolyte transport and accelerates the mobility of catalytic reactants to HER/OER active sites, thereby reducing mass transfer resistance [34].

Scanning electron microscopy (SEM) was used to reveal the

morphology of various catalysts. As shown in Fig. S3a, ZIF-67@NF precursor exhibits hexagonal nanosheets with uniform thickness and independent dense growth. After impregnating NaVO₃ solution, the nanosheet structure is well preserved (Fig. S3b). Noticeably, N-Co₃V₂O₈@NF obtained through nitridation presents thinner and interconnected nanosheets (Fig. 2a), which potentially enhances the exposure of active sites and hastens mass transfer [35]. Transmission electron microscopy (TEM) was performed to in-depth investigate the microstructure of N-Co₃V₂O₈@NF. As presented in Fig. 2b, the TEM image further reveals the nanosheet features of N-Co₃V₂O₈@NF. The high-resolution TEM (HR-TEM) image further reveals distinct lattice fringes with interplanar spacings of 0.254 nm and 0.301 nm, aligning with the (122) and (002) planes of N-Co₃V₂O₈@NF, respectively (Fig. 2c). The selected area electron diffraction (SAED) image validates the single crystalline nature of N-Co₃V₂O₈@NF [36], with the (122) and (002) planes being evident, aligning with the HR-TEM outcomes (Fig. S5a). Moreover, atomic force microscopy (AFM) was used to measure the thickness of N-Co₃V₂O₈@NF nanosheets. As displayed in Fig. 2d-e, the thickness of N-Co₃V₂O₈@NF is approximately 13 nm, which is advantageous to the transport of electrons and protons [37]. Additionally, the nanosheet structure is further verified by high-angle annular dark-field scanning TEM (HAADF-STEM), and elemental mappings show that the Co, V, N, and O elements are uniformly distributed throughout the entire nanosheet (Fig. 2f).

X-ray photoelectron spectroscopy (XPS) was employed to identify the elemental composition and chemical valence states of the catalysts. The XPS survey spectra obviously indicate the evident presence of Co, V, N, O, and C elements in the N-Co₃V₂O₈@NF aligns well with the elemental mappings and EDS patterns showcased in Fig. S5b and Fig. S6a. The C 1s spectrum of N-Co₃V₂O₈@NF was calibrated as C=C (284.0 eV), C-C (284.8 eV), C-O (286.0 eV) and -O-C=O (288.0 eV), respectively (Fig. S6b). As proved in the high-resolution spectra of Co 2p (Fig. 3a), the peaks at 779.9 and 781.7 eV can be indexed to Co³⁺ 2p_{3/2} and Co²⁺ 2p_{3/2}, respectively [38,39]. Notably, a peak discerned at 777.9 eV in the N-Co₃V₂O₈@NF is indicative of the presence of Co-N bonds [40], validating the successful incorporation of nitrogen and the genesis of Co-N active sites. In Fig. 3b, the V 2p spectra revealed the existence of two double peaks at 516.2/523.6 eV and 517.3/524.7 eV, which correspond to V⁴⁺ and V⁵⁺, respectively [41]. Additionally, the new peaks at 514.7 and 522.1 eV in N-Co₃V₂O₈@NF represent the V-N bonds,

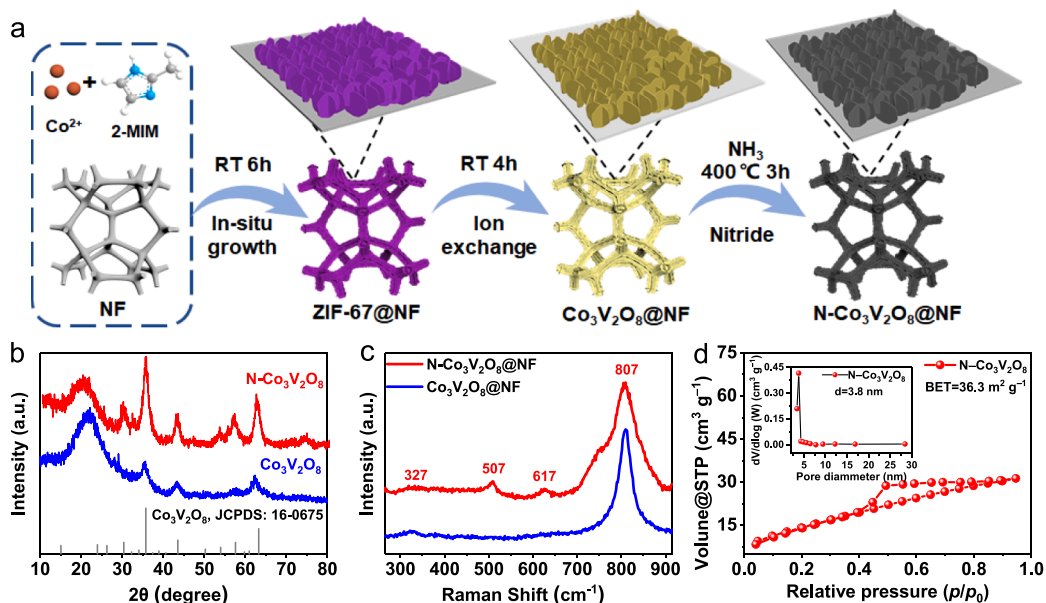


Fig. 1. (a) Schematic illustration of the synthesis of N-Co₃V₂O₈@NF. (b) XRD patterns of N-Co₃V₂O₈ and Co₃V₂O₈. (c) Raman spectra of N-Co₃V₂O₈@NF and Co₃V₂O₈@NF. (d) N₂ adsorption-desorption isotherms and pore-size distribution curves of N-Co₃V₂O₈@NF.

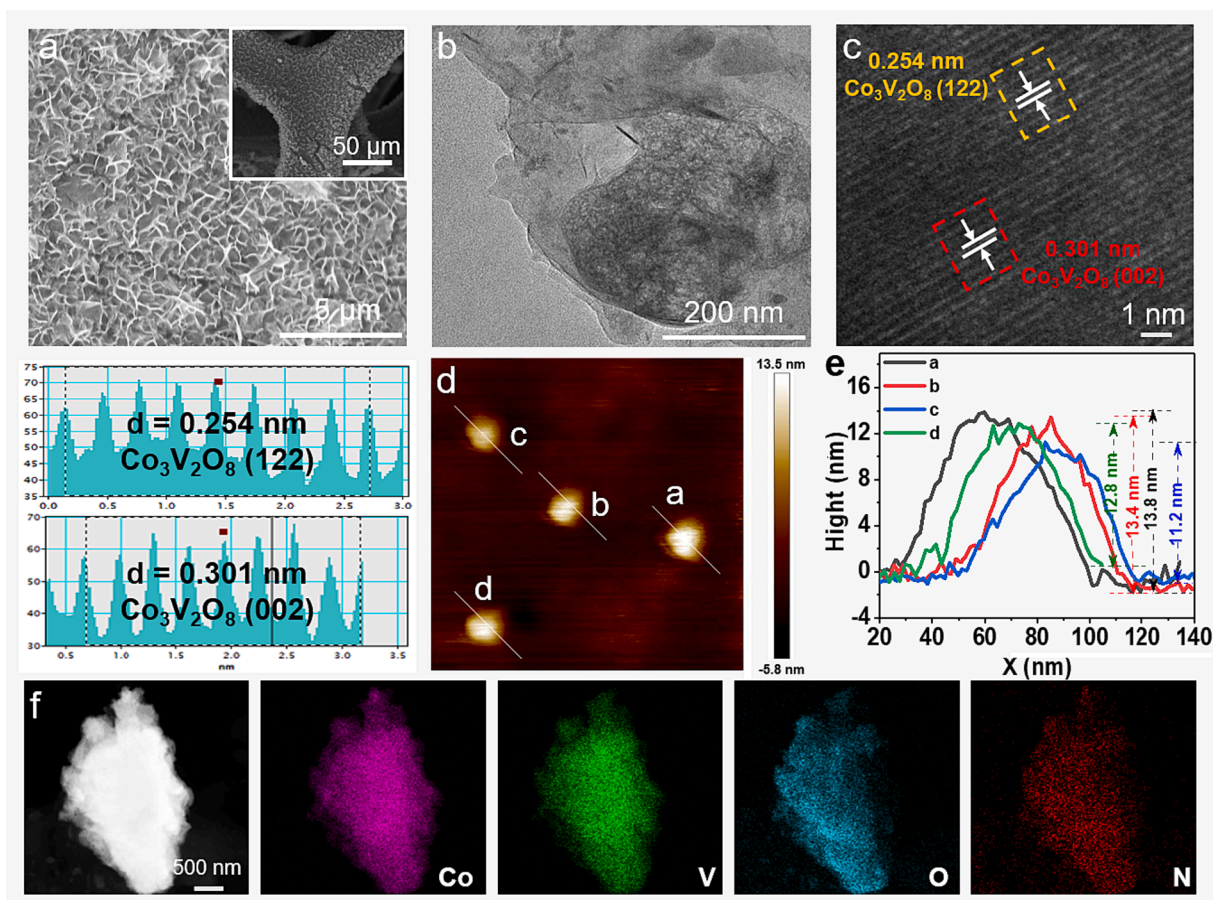


Fig. 2. (a) SEM image of N- $\text{Co}_3\text{V}_2\text{O}_8$ @NF (inset: the lower magnification SEM image). (b) low-magnification TEM image, (c) HR-TEM and the corresponding lattice spacing profiles of the dotted line regions, (d-e) AFM image and the corresponding height profiles, and (f) HAADF-STEM image and EDS elemental mappings of Co, V, O and N of N- $\text{Co}_3\text{V}_2\text{O}_8$ @NF.

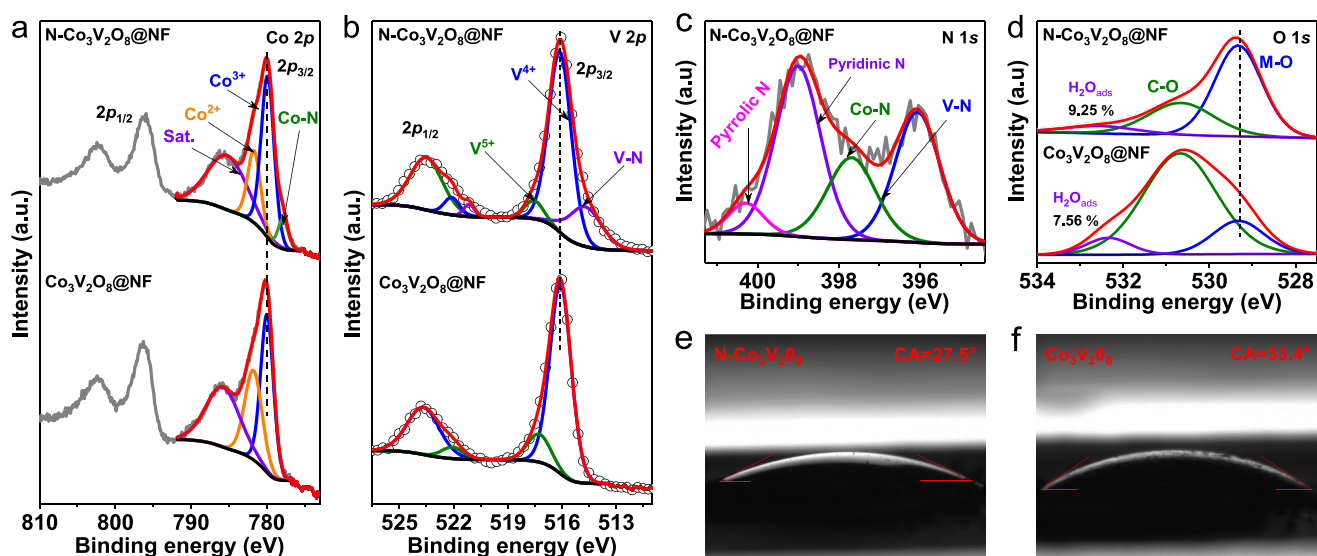


Fig. 3. High-resolution X-ray photoelectron spectra (XPS) of (a) Co 2p and (b) V 2p of N- $\text{Co}_3\text{V}_2\text{O}_8$ @NF and $\text{Co}_3\text{V}_2\text{O}_8$ @NF. (c) N 1s and (d) O 1s of N- $\text{Co}_3\text{V}_2\text{O}_8$ @NF, respectively. (e-f) Contact angle images of N- $\text{Co}_3\text{V}_2\text{O}_8$ and $\text{Co}_3\text{V}_2\text{O}_8$.

reinforcing the successful nitrogen doping in $\text{Co}_3\text{V}_2\text{O}_8$ @NF during nitridation and pointing to the genesis of V-N active sites [42]. The high-resolution N 1s spectrum (Fig. 3c) of N- $\text{Co}_3\text{V}_2\text{O}_8$ @NF can be deconvoluted into four peaks located at 396.1, 397.6, 399.1 and 400.2 eV, which

are ascribed to the V-N bonds, Co-N bonds, pyridinic N, and pyrrolic N, respectively [43,44]. The coexistence of V-N and Co-N bonds epitomizes the effective coordination of nitrogen with Co and V [32,45], further underscoring the dual active sites formed from Co-N and V-N [46].

Meanwhile, the O 1s XPS spectrum of N-Co₃V₂O₈@NF is presented in Fig. 3d, the peaks located at 529.4, 530.7, and 532.2 eV of the obtained electrocatalysts are ascribed to metal–oxygen (M–O) bonds, carbon–oxygen (C–O), and adsorbed water molecules (H₂O_{ads}), respectively [47,48]. Compared with Co₃V₂O₈@NF, the intensity of the surface adsorbed water molecules in N-Co₃V₂O₈@NF apparently increases, indicating an improved hydrophilicity after N doping. To further confirm the hydrophilic feature, the contact angle (CA) test was performed in Fig. 3e–f. Obviously, the contact angle is reduced by 5.90° after N doping, indicating the improved hydrophilicity [49,50]. Therefore, N doping adeptly regulates the electronic structure of Co₃V₂O₈@NF that generates Co–N/V–N dual active sites, and improves its hydrophilicity, thereby enhancing the catalytic performance.

3.2. Electrochemical HER performance evaluation

The hydrogen evolution reaction (HER) efficiency of the devised catalysts was assessed by employing a standard three-electrode setup in a 1.0 M KOH medium. As described in Fig. S7–8, N-Co₃V₂O₈@NF exhibits the optimal catalytic performance when nitrated at 400 °C. Hence, all subsequent discussions and analyses are based on the optimal synthesis condition.

Linear sweep voltammetry (LSV) curves of different catalysts with *iR* compensation calibration are shown in Fig. 4a. The N-Co₃V₂O₈@NF catalyst only requires a low overpotential of 63 mV to drive a current density of 10 mA cm⁻², which outperforms other comparative catalysts and most HER catalysts in literature (Fig. 4b–c and Table S1). Tafel slopes were calculated to gain insight into the reaction mechanism, and the results indicate that N-Co₃V₂O₈@NF exhibits the fastest HER reaction kinetics among the mentioned catalysts (Fig. 4d). Furthermore, we observed a lower *R*_{ct} for N-Co₃V₂O₈@NF compared to all control samples, indicating a reduced resistance at the electrode–electrolyte interface, facilitating rapid electron transfer kinetics (Fig. S9) [51]. Electrochemical measurements were evaluated the electrochemical double-layer capacitance (*C*_{dl}) in the non-faradaic region at different scan rates (Fig. S10). It was observed that N-Co₃V₂O₈@NF has

significantly higher *C*_{dl} value (39.33 mF cm⁻²) than that of Co₃V₂O₈@NF (12.19 mF cm⁻²), N-NaVO₃@NF (3.97 mF cm⁻²) and N-ZIF-67@NF (8.89 mF cm⁻²) (Fig. 4e), which illustrated that N-Co₃V₂O₈@NF was capable of exposing more active sites for HER [52]. This can be attributed to the generation of Co–N and V–N dual active sites, which can provide more active sites. Furthermore, the polarization curve of the N-Co₃V₂O₈@NF catalyst after 1000 consecutive CV cycles almost overlaps with the original one and demonstrates robust durability over 200 h at current density of 10 mA cm⁻² (Fig. 4f inset and Fig. 4f). Meanwhile, the morphology and surface chemical composition of N-Co₃V₂O₈@NF were scrutinized through SEM and XPS, respectively (Fig. S11 and Fig. S12). The morphological structure and chemical state of N-Co₃V₂O₈@NF remain unchanged after a long-term stability test, further demonstrating its excellent stability for HER.

3.3. Electrochemical OER performance evaluation

The self-supported catalyst N-Co₃V₂O₈@NF was directly used as the working electrode to evaluate its OER catalytic activity in 1.0 M KOH. Fig. 5a shows that N-Co₃V₂O₈@NF achieves the lowest overpotential of 256 mV to afford a current density of 10 mA cm⁻², which is superior to Co₃V₂O₈@NF (318 mV), N-NaVO₃@NF (349 mV) and N-ZIF-67@NF (354 mV). Intriguingly, N-Co₃V₂O₈@NF even outperforms the comparative catalysts at 50 and 100 mA cm⁻² (Fig. 5b). The N-Co₃V₂O₈@NF exhibits the smaller Tafel slope (Fig. 5c), demonstrating that N-Co₃V₂O₈@NF proceeds a faster OER kinetics. More importantly, the exceptional OER performance of N-Co₃V₂O₈@NF precedes that of most recently reported OER catalysts (Fig. 5d and Table S2). N-Co₃V₂O₈@NF exhibits the lowest charge transfer resistance (*R*_{ct}) (Fig. 5e), indicating that N-Co₃V₂O₈@NF possesses the fastest electron transfer during OER and that nitrogen incorporation is beneficial for improving electrical conductivity. For assessing durability, a chronopotentiometry test was conducted. As visualized in Fig. 5f, the polarization curves of the N-Co₃V₂O₈@NF catalyst after 1000 consecutive CV cycles closely mirrored the original curve, confirming its capability to maintain stability for an extended period of 300 h at a current density of 10 mA cm⁻². The

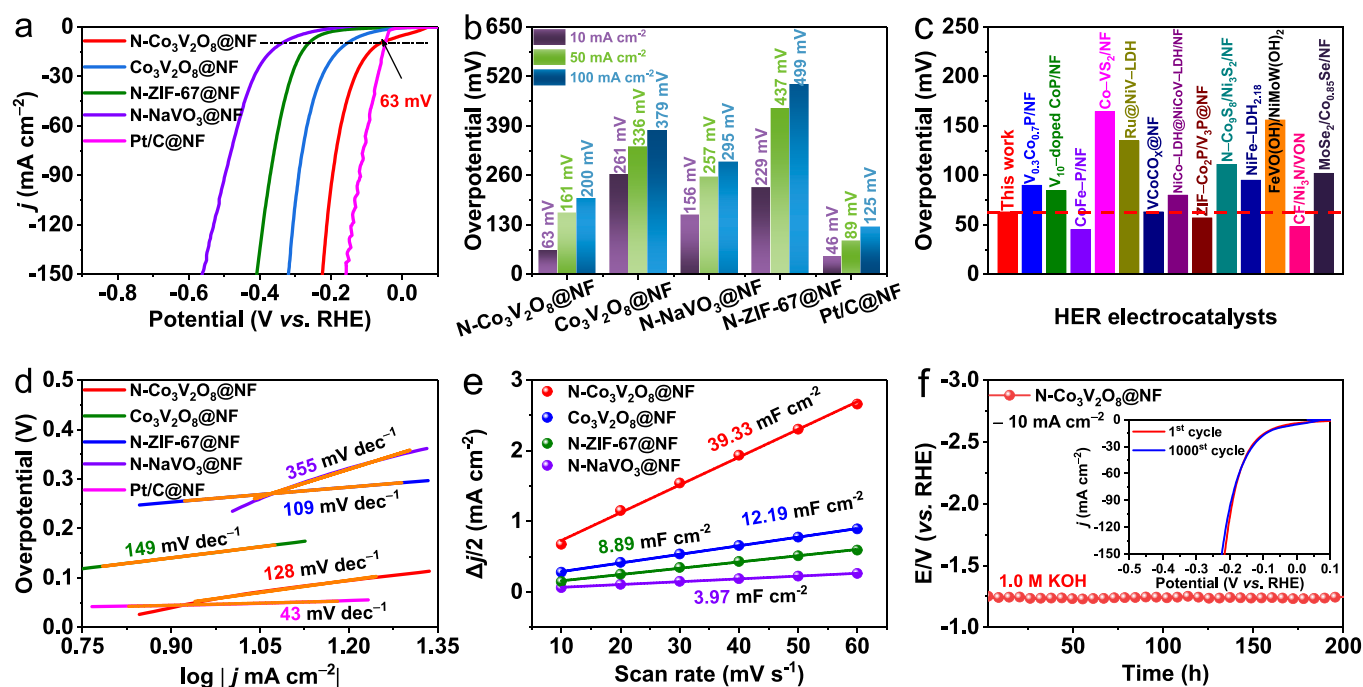


Fig. 4. HER performance of different catalysts in 1.0 M KOH. (a) LSV polarization curves at a scan rate of 2 mV s⁻¹. (b) Comparison of the overpotential at 10, 50, and 100 mA cm⁻². (c) Comparison of overpotential at 10 mA cm⁻² with previously reported catalysts. (d) Tafel slope. (e) Double-layer capacitance (*C*_{dl}) plots. (f) Chronopotentiometry test of N-Co₃V₂O₈@NF at 10 mA cm⁻² (inset: polarization curves of N-Co₃V₂O₈@NF before and after 1000 cycles).

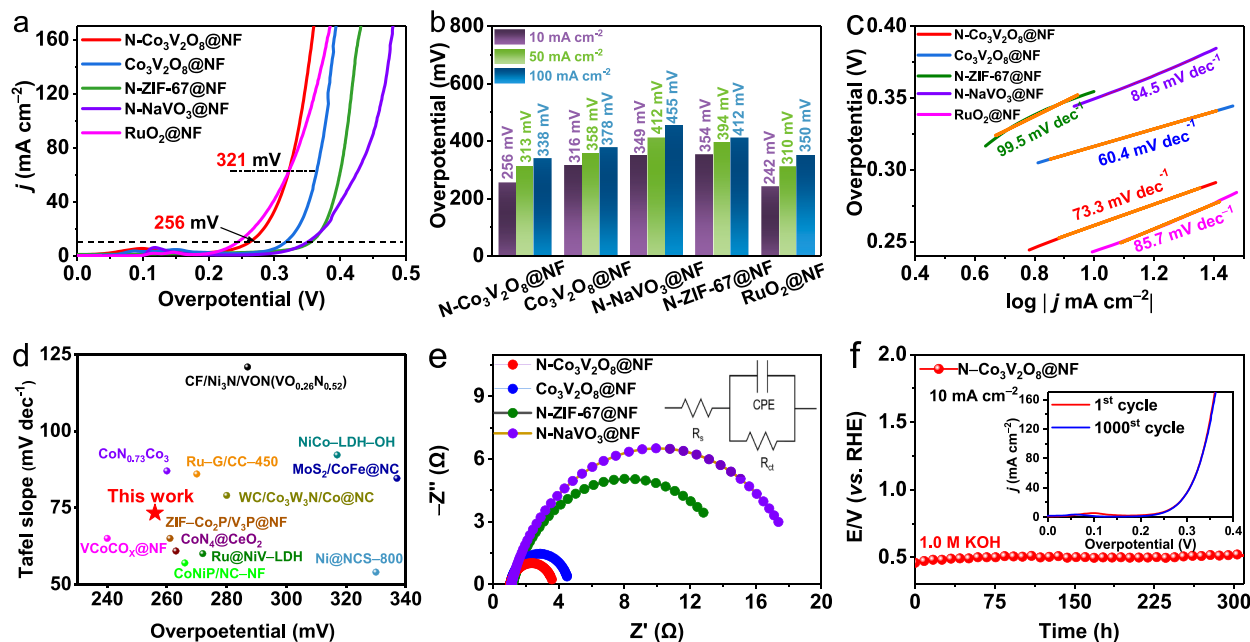


Fig. 5. OER performance of different catalysts in 1.0 M KOH. (a) LSV polarization curves at a scan rate of 2 mV s^{-1} . (b) Comparison of the overpotential at 10, 50, and 100 mA cm^{-2} . (c) Tafel slope. (d) Comparison of overpotential at 10 mA cm^{-2} and Tafel slope with previously reported catalysts. (e) Electrochemical impedance spectroscopy (EIS) data for prepared catalysts. (f) Chronopotentiometry test of $\text{N-Co}_3\text{V}_2\text{O}_8\text{@NF}$ at 10 mA cm^{-2} (inset: polarization curves of $\text{N-Co}_3\text{V}_2\text{O}_8\text{@NF}$ before and after 1000 cycles).

morphological characteristics and surface chemical states of the catalyst were characterized by SEM and XPS after the OER stability test. The SEM results show that the catalyst maintains its intact nanosheet structure (Fig. S13), demonstrating excellent stability. Interestingly, there are slight changes observed in the chemical composition of the catalyst surface. Fig. S14 displays that the disappearance of the Co-N and V-N bonds in the catalyst, while the content of Co^{3+} and V^{5+} increases significantly, which is attributed to the oxidation reaction during the

OER process [53]. These findings emphasize that the synergy between Co-N and V-N plays a pivotal role in fostering active sites during the OER.

3.4. Electrochemical OWS performance evaluation

As previously noted, $\text{N-Co}_3\text{V}_2\text{O}_8\text{@NF}$ exhibits outstanding electrocatalytic activity and durability for HER and OER, marking it as a

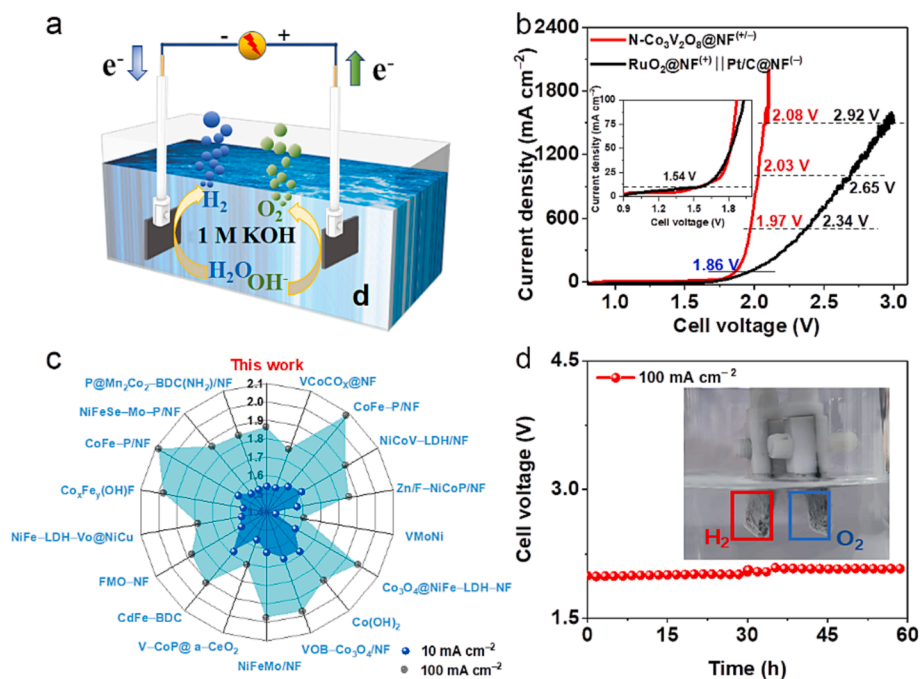


Fig. 6. (a) Schematic diagram of the two-electrode OWS system. (b) Polarization curves of $\text{N-Co}_3\text{V}_2\text{O}_8\text{@NF}^{(+/-)}$ and $\text{RuO}_2\text{@NF}^{(+)} \parallel \text{Pt/C@NF}^{(-)}$. (c) Comparison of the cell voltages at current densities of 10 and 100 mA cm^{-2} with previously reported catalysts. (d) Chronopotentiometry curve at a current density of 100 mA cm^{-2} for $\text{N-Co}_3\text{V}_2\text{O}_8\text{@NF}^{(+/-)}$ (inset: a digital photograph of the two-electrode OWS system).

potential catalyst for overall water splitting (OWS). To rigorously evaluate its performance in an OWS system, a two-electrode OWS setup was carried out with N-Co₃V₂O₈@NF as both the anode and cathode (Fig. 6a). As presented in Fig. 6b, the N-Co₃V₂O₈@NF^(+/-) system (1.54 V@10 mA cm⁻²/1.86 V@100 mA cm⁻²) achieves comparable performance to RuO₂@NF⁽⁺⁾ || Pt/C@NF⁽⁻⁾ (1.54 V@10 mA cm⁻²/1.86 V@100 mA cm⁻²). Notably, the assembled N-Co₃V₂O₈@NF^(+/-) electrolyzer exhibits remarkably low cell voltages of 1.97 V, 2.03 V, and 2.08 V at high current densities of 500, 1000, and 1500 mA cm⁻², highlighting its substantial potential for industrial applications. In a broader context, when benchmarked against several documented catalysts, the OWS efficiency of N-Co₃V₂O₈@NF consistently emerges superior (Fig. 6c and Table S3). A critical parameter for industrial viability is the stability of the system. In this regard, the N-Co₃V₂O₈@NF^(+/-) system shines, demonstrating unwavering performance at a hefty 100 mA cm⁻² for an extended period of 60 h, maintaining a consistent voltage and continuously producing gas bubbles (Fig. 6d). This consistent performance underscores its remarkable durability and positions N-Co₃V₂O₈@NF as a front-runner in the OWS system.

As noted earlier, the standout performance of N-Co₃V₂O₈@NF across HER, OER, and OWS operations can be attributed to a confluence of strategic enhancements and material attributes. These key factors can be ascribed to the following aspects: (1) Advanced nanosheet architecture: The interlinked nanosheet structure can significantly increase the specific surface area, and facilitate efficient electrolyte transport and gas emission [54,55]. (2) Bimetallic active sites: The bimetallic site combination of Co-N and V-N not only multiplies the number of active sites but also synergistically boosts their individual catalytic activity efficiency [41]. (3) Nitrogen doping and electronic modulation: N doping can effectively modulate the electronic structure of the metal centers, which is conducive to improving the electrical conductivity and optimizing the adsorption of reaction intermediates, thereby improving the intrinsic activity of the catalyst [56]. (4) Self-supporting electrode design: The prepared self-supporting binder-free electrode can reduce the electrode resistance and accelerate the electron transport during electrocatalysis [57]. (5) Hydrophilicity enhancements: N doping can effectively modulate the hydrophilicity of the electrocatalytic material, provide a more potent capillary force stronger capillary force, promote contact between the active site and reactants, and pave the way for faster reaction kinetics [50,58].

4. Conclusion

In summary, we present the crucial promotion of Co-N and V-N dual active sites on the HER and OER activity. The as-prepared N-Co₃V₂O₈@NF achieves lower overpotentials of 63 and 256 mV at 10 cm⁻² for HER and OER, respectively, with remarkable long-term stability. Additionally, the assembled N-Co₃V₂O₈@NF^(+/-) electrolyzer demonstrates a need for lower cell voltages to achieve higher current densities (500–1500 mA cm⁻²), surpassing the performance of RuO₂@NF⁽⁺⁾ || Pt/C@NF⁽⁻⁾, thereby presenting significant potential for industrial applications. The superior electrochemical performance is attributed to the staggered nanosheet structure, N-doping and the favorable Co-N/V-N dual active sites, which endow N-Co₃V₂O₈@NF with abundant active sites, enhanced electrical conductivity, accelerated reaction kinetics, and better hydrophilicity. This work provides an insightful blueprint for future endeavors in the design of efficient and bifunctional electrocatalysts with dual active sites, paving the way for next-generation industrial water electrolysis systems.

CRedit authorship contribution statement

Mingcheng Gao: Data curation, Investigation, Writing – original draft. **Zhiyang Huang:** Investigation, Methodology. **Lixia Wang:** Data curation, Methodology. **Huatong Li:** Data curation. **Changping Ruan:** Supervision. **Raeid Sadeq:** Writing – review & editing. **Tayirjan Taylor**

Isimjan: Writing – review & editing. **Xiulin Yang:** Supervision, Writing – review & editing.

Declaration of competing interest

The authors declare that they have no known competing financial interests or personal relationships that could have appeared to influence the work reported in this paper.

Data availability

The data that has been used is confidential.

Acknowledgements

This work has been supported by the National Natural Science Foundation of China (no. 21965005, 52363028), Natural Science Foundation of Guangxi Province (2021GXNSFAA076001), and Guangxi Technology Base and Talent Subject (GUIKE AD18126001, GUIKE AD20297039).

Appendix A. Supplementary material

Supplementary data to this article can be found online at <https://doi.org/10.1016/j.jcis.2023.12.064>.

References

- [1] L. Liardet, X. Hu, Amorphous cobalt vanadium oxide as a highly active electrocatalyst for oxygen evolution, *ACS Catal.* 8 (2018) 644–650, <https://doi.org/10.1021/acscatal.7b03198>.
- [2] Q. Gao, W. Zhang, Z. Shi, L. Yang, Y. Tang, Structural design and electronic modulation of transition-metal-carbide electrocatalysts toward efficient hydrogen evolution, *Adv. Mater.* 31 (2019), e1802880, <https://doi.org/10.1002/adma.201802880>.
- [3] J. Wang, H. Kong, J. Zhang, Y. Hao, Z. Shao, F. Ciucci, Carbon-based electrocatalysts for sustainable energy applications, *Prog. Mater. Sci.* 116 (2021), 100717, <https://doi.org/10.1016/j.pmatsci.2020.100717>.
- [4] K. Chakrapani, G. Bendt, H. Hajiyani, T. Lunkenbein, M.T. Greiner, L. Masliuk, S. Salamon, J. Landers, R. Schlögl, H. Wende, R. Pentcheva, S. Schulz, M. Behrens, The role of composition of uniform and highly dispersed cobalt vanadium iron spinel nanocrystals for oxygen electrocatalysis, *ACS Catal.* 8 (2018) 1259–1267, <https://doi.org/10.1021/acscatal.7b03529>.
- [5] J. Yu, Q. He, G. Yang, W. Zhou, Z. Shao, M. Ni, Recent advances and prospective in ruthenium-based materials for electrochemical water splitting, *ACS Catal.* 9 (2019) 9973–10011, <https://doi.org/10.1021/acscatal.9b02457>.
- [6] Y. Li, Y. Sun, Y. Qin, W. Zhang, L. Wang, M. Luo, H. Yang, S. Guo, Recent advances on water-splitting electrocatalysis mediated by noble-metal-based nanostructured materials, *Adv. Energy Mater.* 10 (2020) 1903120, <https://doi.org/10.1002/aenm.201903120>.
- [7] M.I. James, Recent progress on earth abundant hydrogen evolution reaction and oxygen evolution reaction bifunctional electrocatalyst for overall water splitting in alkaline media, *J. Power Sources* 333 (2016) 213–236, <https://doi.org/10.1016/j.jpowsour.2016.09.161>.
- [8] J. Hou, Y. Wu, B. Zhang, S. Cao, Z. Li, L. Sun, Rational design of nanoarray architectures for electrocatalytic water splitting, *Adv. Funct. Mater.* 29 (2019) 1808367, <https://doi.org/10.1002/adfm.201808367>.
- [9] G. Zhou, Z. Guo, Y. Shan, S. Wu, J. Zhang, K. Yan, L. Liu, P.K. Chu, X. Wu, High-efficiency hydrogen evolution from seawater using hetero-structured T/Td phase ReS₂ nanosheets with cationic vacancies, *Nano Energy* 55 (2019) 42–48, <https://doi.org/10.1016/j.nanoen.2018.10.047>.
- [10] G. Fu, X. Yan, Y. Chen, L. Xu, D. Sun, J.M. Lee, Y. Tang, Boosting bifunctional oxygen electrocatalysis with 3D graphene aerogel-supported Ni/MnO particles, *Adv. Mater.* 30 (2018) 1704609, <https://doi.org/10.1002/adma.201704609>.
- [11] S.H. Ye, Z.X. Shi, J.X. Feng, Y.X. Tong, G.R. Li, Activating CoOOH porous nanosheet arrays by partial iron substitution for efficient oxygen evolution reaction, *Angew. Chem. Int. Ed.* 57 (2018) 2672–2676, <https://doi.org/10.1002/anie.201712549>.
- [12] H. Wang, J. Li, K. Li, Y. Lin, J. Chen, L. Gao, V. Nicolosi, X. Xiao, J.M. Lee, Transition metal nitrides for electrochemical energy applications, *Chem. Soc. Rev.* 50 (2021) 1354–1390, <https://doi.org/10.1039/d0cs00415d>.
- [13] X. Huang, X. Xu, X. Luan, D. Cheng, CoP nanowires coupled with CoMoP nanosheets as a highly efficient cooperative catalyst for hydrogen evolution reaction, *Nano Energy* 68 (2020), 104332, <https://doi.org/10.1016/j.nanoen.2019.104332>.

- [14] Y. Yang, R. Zeng, Y. Xiong, F.J. DiSalvo, H.D. Abruna, Cobalt-based nitride-core oxide-shell oxygen reduction electrocatalysts, *J. Am. Chem. Soc.* 141 (2019) 19241–19245, <https://doi.org/10.1021/jacs.9b10809>.
- [15] E. Fabbri, A. Haberer, K. Waltar, R. Kötz, T.J. Schmidt, Developments and perspectives of oxide-based catalysts for the oxygen evolution reaction, *Catal. Sci. Technol.* 4 (2014) 3800–3821, <https://doi.org/10.1039/c4cy00669k>.
- [16] M. Xing, L.-B. Kong, M.-C. Liu, L.-Y. Liu, L. Kang, Y.-C. Luo, Cobalt vanadate as highly active, stable, noble metal-free oxygen evolution electrocatalyst, *J. Mater. Chem. A* 2 (2014) 18435–18443, <https://doi.org/10.1039/c4ta03776f>.
- [17] A. Mondal, S. Ganguli, H.R. Inta, V. Mahalingam, Influence of vanadate structure on electrochemical surface reconstruction and OER performance of CoV_2O_6 and $\text{Co}_3\text{V}_2\text{O}_8$, *ACS Appl. Energy Mater.* 4 (2021) 5381–5387, <https://doi.org/10.1021/acsaem.1c00701>.
- [18] C. Yang, W. Zhong, K. Shen, Q. Zhang, R. Zhao, H. Xiang, J. Wu, X. Li, N. Yang, Electrochemically reconstructed Cu-FeOOH/ Fe_3O_4 catalyst for efficient hydrogen evolution in alkaline media, *Adv. Energy Mater.* 12 (2022) 2200077, <https://doi.org/10.1002/aenm.202200077>.
- [19] J. Yu, Z. Li, T. Liu, S. Zhao, D. Guan, D. Chen, Z. Shao, M. Ni, Morphology control and electronic tailoring of Co_xA_y ($A = \text{P}, \text{S}, \text{Se}$) electrocatalysts for water splitting, *Chem. Eng. J.* 460 (2023), 141674, <https://doi.org/10.1016/j.cej.2023.141674>.
- [20] J. Zhang, T. Wang, D. Pohl, B. Rellinghaus, R. Dong, S. Liu, X. Zhuang, X. Feng, Interface engineering of $\text{MoS}_2/\text{Ni}_3\text{S}_2$ heterostructures for highly enhanced electrochemical overall-water-splitting activity, *Angew. Chem. Int. Ed.* 55 (2016) 6702–6707, <https://doi.org/10.1002/anie.201602237>.
- [21] M. Saruyama, C.M. Pelicano, T. Teranishi, Bridging electrocatalyst and cocatalyst studies for solar hydrogen production via water splitting, *Chem. Sci.* 13 (2022) 2824–2840, <https://doi.org/10.1039/d1sc06015e>.
- [22] Y. Men, P. Li, F. Yang, G. Cheng, S. Chen, W. Luo, Nitrogen-doped CoP as robust electrocatalyst for high-efficiency pH-universal hydrogen evolution reaction, *Appl. Catal. B Environ.* 253 (2019) 21–27, <https://doi.org/10.1016/j.apcatb.2019.04.038>.
- [23] L. Zhang, Y. Qi, L. Sun, G. Chen, L. Wang, M. Zhang, D. Zeng, Y. Chen, X. Wang, K. Xu, F. Ma, Facile route of nitrogen doping in nickel cobalt phosphide for highly efficient hydrogen evolution in both acid and alkaline electrolytes, *Appl. Surf. Sci.* 512 (2020), 145715, <https://doi.org/10.1016/j.apsusc.2020.145715>.
- [24] Y. Huang, M. Zheng, Z. Lin, B. Zhao, S. Zhang, J. Yang, C. Zhu, H. Zhang, D. Sun, Y. Shi, Flexible cathodes and multifunctional interlayers based on carbonized bacterial cellulose for high-performance lithium–sulfur batteries, *J. Mater. Chem. A* 3 (2015) 10910–10918, <https://doi.org/10.1039/c5ta01515d>.
- [25] I. Ahmed, C.-U. Kim, S.H. Jhung, Carbon-supported vanadium nitride catalyst, prepared from urea-loaded MIL-100(V) in the absence of external ammonia flow, having good performance in oxidative desulfurization, *J. Clean. Prod.* 384 (2023), 135509, <https://doi.org/10.1016/j.jclepro.2022.135509>.
- [26] H. Wang, M. Cui, G. Fu, J. Zhang, X. Ding, I. Azaceta, M. Bugnet, D. M. Kepaptsoglou, V.K. Lazarov, V.A. de la Peña O’Shea, F.E. Oropeza, K.H. L. Zhang, Vertically aligned Ni/NiO nanocomposites with abundant oxygen deficient hetero-interfaces for enhanced overall water splitting, *Sci. China Chem.* 65 (2022) 1885–1894, <https://doi.org/10.1007/s11426-022-1326-2>.
- [27] Q. Yu, Z. Zhang, S. Qiu, Y. Luo, Z. Liu, F. Yang, H. Liu, S. Ge, X. Zou, B. Ding, W. Ren, H.M. Cheng, C. Sun, B. Liu, A Ta-Ta S_2 monolith catalyst with robust and metallic interface for superior hydrogen evolution, *Nat. Commun.* 12 (2021) 6051, <https://doi.org/10.1038/s41467-021-26315-7>.
- [28] P. Yan, M. Huang, B. Wang, Z. Wan, M. Qian, H. Yan, T.T. Isimjan, J. Tian, X. Yang, Oxygen defect-rich double-layer hierarchical porous Co_3O_4 arrays as high-efficient oxygen evolution catalyst for overall water splitting, *J. Energy Chem.* 47 (2020) 299–306, <https://doi.org/10.1016/j.jechem.2020.02.006>.
- [29] J. Luo, X. Tian, J. Zeng, Y. Li, H. Song, S. Liao, Limitations and improvement strategies for early-transition-metal nitrides as competitive catalysts toward the oxygen reduction reaction, *ACS Catal.* 6 (2016) 6165–6174, <https://doi.org/10.1021/acscatal.6b01618>.
- [30] J. Chen, H. Li, Z. Pei, Q. Huang, Z. Yuan, C. Wang, X. Liao, G. Henkelman, Y. Chen, L. Wei, Catalytic activity atlas of ternary Co–Fe–V metal oxides for the oxygen evolution reaction, *J. Mater. Chem. A* 8 (2020) 15951–15961, <https://doi.org/10.1039/d0ta04088f>.
- [31] X.H. Chen, T. Li, X. Li, J. Lei, N.B. Li, H.Q. Luo, Oxyanion-coordinated co-based catalysts for optimized hydrogen evolution: the feedback of adsorbed anions to the catalytic activity and mechanism, *ACS Catal.* 13 (2023) 6721–6729, <https://doi.org/10.1021/acscatal.3c00598>.
- [32] X. Zhao, Q. Han, J. Li, X. Du, G. Liu, Y. Wang, L. Wu, Z. Chen, Ordered macroporous design of sacrificial Co/VN nano-heterojunction as bifunctional oxygen electrocatalyst for rechargeable zinc-air batteries, *Chem. Eng. J.* 433 (2022), 133509, <https://doi.org/10.1016/j.cej.2021.133509>.
- [33] D. Guo, Z. Zeng, Z. Wan, Y. Li, B. Xi, C. Wang, A CoN-based OER electrocatalyst capable in neutral medium: atomic layer deposition as rational strategy for fabrication, *Adv. Funct. Mater.* 31 (2021) 2101324, <https://doi.org/10.1002/adfm.202101324>.
- [34] M.A. Ahsan, A.R. Puente Santiago, Y. Hong, N. Zhang, M. Cano, E. Rodriguez-Castellon, L. Echegoyen, S.T. Sreenivasan, J.C. Noveron, Tuning of trifunctional NiCu bimetallic nanoparticles confined in a porous carbon Network with surface composition and local structural distortions for the electrocatalytic oxygen reduction, oxygen and hydrogen evolution reactions, *J. Am. Chem. Soc.* 142 (2020) 14688–14701, <https://doi.org/10.1021/jacs.0c06960>.
- [35] X. Qin, B. Yan, D. Kim, Z. Teng, T. Chen, J. Choi, L. Xu, Y. Piao, Interfacial engineering and hydrophilic/aerophobic tuning of $\text{Sn}_4\text{P}_3/\text{Co}_2\text{P}$ heterojunction nanoarrays for high-efficiency fully reversible water electrolysis, *Appl. Catal. B Environ.* 304 (2022), <https://doi.org/10.1016/j.apcatb.2021.120923>.
- [36] H. Jin, X. Liu, A. Vasileff, Y. Jiao, Y. Zhao, Y. Zheng, S.Z. Qiao, Single-crystal nitrogen-rich two-dimensional Mo_5N_6 nanosheets for efficient and stable seawater splitting, *ACS Nano* 12 (2018) 12761–12769, <https://doi.org/10.1021/acsnano.8b07841>.
- [37] M. Zhao, T. Guo, W. Qian, Z. Wang, X. Zhao, L. Wen, D. He, Fe-incorporated cobalt-based metal-organic framework ultrathin nanosheets for electrocatalytic oxygen evolution, *Chem. Eng. J.* 422 (2021), 130055, <https://doi.org/10.1016/j.cej.2021.130055>.
- [38] R. Zhang, Z. Wei, G. Ye, G. Chen, J. Miao, X. Zhou, X. Zhu, X. Cao, X. Sun, “d-Electron Complementation” Induced V-Co Phosphide for Efficient Overall Water Splitting, *Adv. Energy Mater.* 11 (2021) 2101758, <https://doi.org/10.1002/aenm.202101758>.
- [39] C. Jiang, J. Yang, T. Zhao, L. Xiong, Z.-X. Guo, Y. Ren, H. Qi, A. Wang, J. Tang, $\text{Co}^{3+}\text{-O-V}^{4+}$ cluster in CoVO_x nanorods for efficient and stable electrochemical oxygen evolution, *Appl. Catal. B Environ.* 282 (2021), 119571, <https://doi.org/10.1016/j.apcatb.2020.119571>.
- [40] Y. Wu, L. Chen, X. Yang, Y. Li, K. Shen, Facet-selective growth of MOF-on-MOF heterostructures enables etching-free synthesis of highly-open Co/N-doped Carbon nanoframes for efficient catalysis, *Sci. China Chem.* 65 (2022) 2450–2461, <https://doi.org/10.1007/s11426-022-1357-y>.
- [41] Z. Luo, Q. Peng, Z. Huang, L. Wang, Y. Yang, J. Dong, T.T. Isimjan, X. Yang, Fine-tune d-band center of cobalt vanadium oxide nanosheets by N-doping as a robust overall water splitting electrocatalyst, *J. Colloid Interface Sci.* 629 (2022) 111–120, <https://doi.org/10.1016/j.jcis.2022.09.069>.
- [42] D. Liu, H. Ai, J. Li, M. Fang, M. Chen, D. Liu, X. Du, P. Zhou, F. Li, K.H. Lo, Y. Tang, S. Chen, L. Wang, G. Xing, H. Pan, Surface reconstruction and phase transition on vanadium–cobalt–iron trimetal nitrides to form active oxyhydroxide for enhanced electrocatalytic water oxidation, *Adv. Energy Mater.* 10 (2020) 2002464, <https://doi.org/10.1002/aenm.202002464>.
- [43] Z. Li, H. He, H. Cao, S. Sun, W. Diao, D. Gao, P. Lu, S. Zhang, Z. Guo, M. Li, R. Liu, D. Ren, C. Liu, Y. Zhang, Z. Yang, J. Jiang, G. Zhang, Atomic Co/Ni dual sites and Co/Ni alloy nanoparticles in N-doped porous Janus-like carbon frameworks for bifunctional oxygen electrocatalysis, *Appl. Catal. B Environ.* 240 (2019) 112–121, <https://doi.org/10.1016/j.apcatb.2018.08.074>.
- [44] X. Gao, Y. Yu, Q. Liang, Y. Pang, L. Miao, X. Liu, Z. Kou, J. He, S.J. Pennycook, S. Mu, J. Wang, Surface nitridation of nickel–cobalt alloy nanocactoids raises the performance of water oxidation and splitting, *Appl. Catal. B Environ.* 270 (2020), 118889, <https://doi.org/10.1016/j.apcatb.2020.118889>.
- [45] P. Zhou, D. Xing, Y. Liu, Z. Wang, P. Wang, Z. Zheng, X. Qin, X. Zhang, Y. Dai, B. Huang, Accelerated electrocatalytic hydrogen evolution on non-noble metal containing trinickel nitride by introduction of vanadium nitride, *J. Mater. Chem. A* 7 (2019) 5513–5521, <https://doi.org/10.1039/c8ta12043a>.
- [46] Y. Wang, D. Liu, Z. Liu, C. Xie, J. Huo, S. Wang, Porous cobalt-iron nitride nanowires as excellent bifunctional electrocatalysts for overall water splitting, *Chem. Commun.* 52 (2016) 12614–12617, <https://doi.org/10.1039/c6cc06608a>.
- [47] Y. Hu, Z. Huang, Q. Zhang, T. Taylor Isimjan, Y. Chu, Y. Mu, B. Wu, Z. Huang, X. Yang, L. Zeng, Interfacial engineering of $\text{Co}_{5.47}\text{N}/\text{Mo}_5\text{N}_6$ nanosheets with rich active sites synergistically accelerates water dissociation kinetics for Pt-like hydrogen evolution, *J. Colloid Interface Sci.* 643 (2023) 455–464, <https://doi.org/10.1016/j.jcis.2023.04.028>.
- [48] S. Dou, S. Zhou, H. Huang, P. Yan, E. Shoko, T.T. Isimjan, X. Yang, Metal-organic framework (MOF)-derived electron-transfer enhanced homogeneous PdO-Rich Co_3O_4 as a highly efficient bifunctional catalyst for sodium borohydride hydrolysis and 4-nitrophenol reduction, *Chem. Eur. J.* 26 (2020) 16923–16931, <https://doi.org/10.1002/chem.202003793>.
- [49] M. Yu, Z. Wang, J. Liu, F. Sun, P. Yang, J. Qiu, A hierarchically porous and hydrophilic 3D nickel–iron/MXene electrode for accelerating oxygen and hydrogen evolution at high current densities, *Nano Energy* 63 (2019), 103880, <https://doi.org/10.1016/j.nanoen.2019.103880>.
- [50] W. Xie, T. Yu, Z. Ou, J. Zhang, R. Li, S. Song, Y. Wang, Self-supporting clusters constituted of nitrogen-doped CoMoO_4 nanosheets for efficiently catalyzing the hydrogen evolution reaction in alkaline media, *ACS Sustain. Chem. Eng.* 8 (2020) 9070–9078, <https://doi.org/10.1021/acssuschemeng.0c02283>.
- [51] J. Zhao, X. Ren, X. Sun, Y. Zhang, Q. Wei, X. Liu, D. Wu, In situ evolution of surface Co_2CrO_4 to $\text{CoOOH}/\text{CrOOH}$ by electrochemical method: toward boosting electrocatalytic water oxidation, *Chin. J. Catal.* 42 (2021) 1096–1101, [https://doi.org/10.1016/S1872-2067\(20\)63730-5](https://doi.org/10.1016/S1872-2067(20)63730-5).
- [52] J. Wu, R. Zhao, H. Xiang, C. Yang, W. Zhong, C. Zhang, Q. Zhang, X. Li, N. Yang, Exposing highly active (100) facet on a $\text{SnS}_2/\text{SnO}_2$ electrocatalyst to boost efficient hydrogen evolution, *Appl. Catal. B Environ.* 292 (2021), 120200, <https://doi.org/10.1016/j.apcatb.2021.120200>.
- [53] X. Shao, Y. Yang, Y. Liu, P. Yan, S. Zhou, T. Taylor Isimjan, X. Yang, Oxygen vacancy-rich N-doped carbon encapsulated BiOCl-CNTs heterostructures as robust electrocatalyst synergistically promote oxygen reduction and Zn-air batteries, *J. Colloid Interface Sci.* 607 (2022) 826–835, <https://doi.org/10.1016/j.jcis.2021.08.210>.
- [54] Y. Lu, Z. Li, Y. Xu, L. Tang, S. Xu, D. Li, J. Zhu, D. Jiang, Bimetallic Co-Mo nitride nanosheet arrays as high-performance bifunctional electrocatalysts for overall

- water splitting, Chem. Eng. J. 411 (2021), 128433, <https://doi.org/10.1016/j.cej.2021.128433>.
- [55] B. Zhang, H. Xu, Q. Chen, H. Chen, G. He, ZIF-67 derived Mo₂N/Mo₂C heterostructure as high-efficiency electrocatalyst for hydrogen evolution reaction, J. Alloys Compd. 922 (2022), 166216, <https://doi.org/10.1016/j.jallcom.2022.166216>.
- [56] T. Xiong, J. Li, J. Chandra Roy, M. Koroma, Z. Zhu, H. Yang, L. Zhang, T. Ouyang, M.S. Balogun, M. Al-Mamun, Hetero-interfacial nickel nitride/vanadium oxynitride porous nanosheets as trifunctional electrodes for HER, OER and sodium ion batteries, J. Energy Chem. 81 (2023) 71–81, <https://doi.org/10.1016/j.jechem.2023.01.064>.
- [57] H. Yu, L. Wang, H. Li, Z. Luo, T.T. Isimjan, X. Yang, Improving the electrocatalytic activity of a nickel-organic framework toward the oxygen evolution reaction through vanadium doping, Chem. Eur. J. 28 (2022), e202201784, <https://doi.org/10.1002/chem.202201784>.
- [58] M. Guo, Z. Huang, Y. Qu, L. Wang, H. Li, T.T. Isimjan, X. Yang, Synergistic effect and nanostructure engineering of three-dimensionally hollow mesoporous spherical Cu₃P/TiO₂ in aqueous/flexible Zn–air batteries, Appl. Catal. B Environ. 320 (2023), <https://doi.org/10.1016/j.apcatb.2022.121991>.